

Supplementary Information for:

**Crystalline curcumin bioMOF obtained by precipitation in supercritical CO₂
and structural determination by electron diffraction tomography**

Nuria Portolés-Gil,^a Arianna Lanza,^b Núria Aliaga-Alcalde,^{a,c} José Antonio Ayllón,^d Mauro Gemmi,^b Enrico Mugnaioli,^{b,*} Ana M. López-Periago,^{a,*} Concepción Domingo^{a,*}

^a *Instituto de Ciencia de Materiales de Barcelona (ICMAB-CSIC), Campus UAB s/n, Bellaterra 08193, Spain*

^b *Center for Nanotechnology Innovation@NEST, Istituto Italiano di Tecnologia, Piazza San Silvestro 12, 56127 Pisa, Italy*

^c *ICREA, Institució Catalana de Recerca i Estudis Avançats, Passeig Lluís Companys 23, 08010 Barcelona, Spain*

^d *Departamento de Química Analítica, Universidad de Barcelona, Martí i Franques 1–11, 08028 Barcelona, Spain*

* *Corresponding author: conchi@icmab.es*

Supporting Information includes 12 pages, two tables and 10 figures.

Reagents behavior in scCO₂

XRD analysis

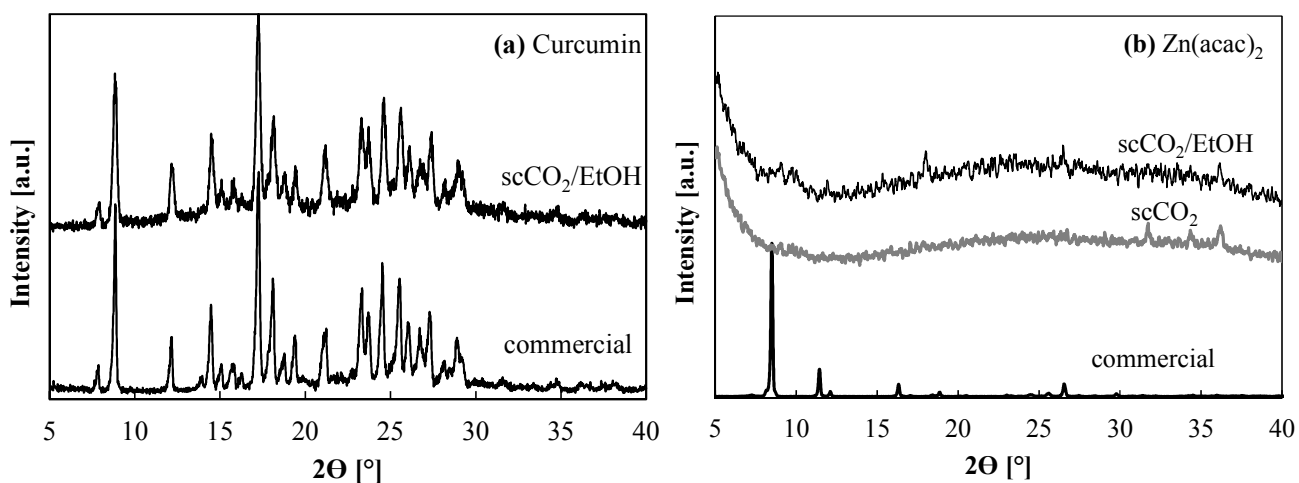


Figure S1. Powder XRD structural characterization of reagents before and after supercritical treatment: (a) CCM, and (b) Zn(acac)₂.

Infrared analysis. The ATR-FTIR spectra of the raw and treated CCM samples (Fig. S2a) revealed the presence of the most characteristic peaks of curcumin. In them, the stretching region of hydroxyl moieties appears as a broad band in the range of 3100-3600 cm⁻¹. Signals at 2950, 2850, 1512, 1350 and 962 cm⁻¹ relate to C-H vibrations. The strong signal at 1626 cm⁻¹ is described as having a (C=C)/(C=O) mixed character. The nearby sharp peak at 1602 cm⁻¹ is attributed to symmetric aromatic C=C stretching vibrations. The peak at 1506 cm⁻¹ relates to C=O, while the enol C-O and the C-O-C vibrations are observed at 1280 cm⁻¹ and 1026 cm⁻¹, respectively. The prominent peaks in the ATR-FTIR spectrum of hydrated Zn(acac)₂ (Fig. S2b) are described as follows: a broad band centered at 3190 cm⁻¹, that indicates water present in the precursor; C-H signals at 3000, 2920 and 1188 cm⁻¹; C=C & C=O peaks at 1592 cm⁻¹ in addition to C=O & C-H at 1446 cm⁻¹; CH₃ at 1392, 1360 and 1017 cm⁻¹; C-C at 1258 cm⁻¹; and C-CH₃ at 932 and 655 cm⁻¹.

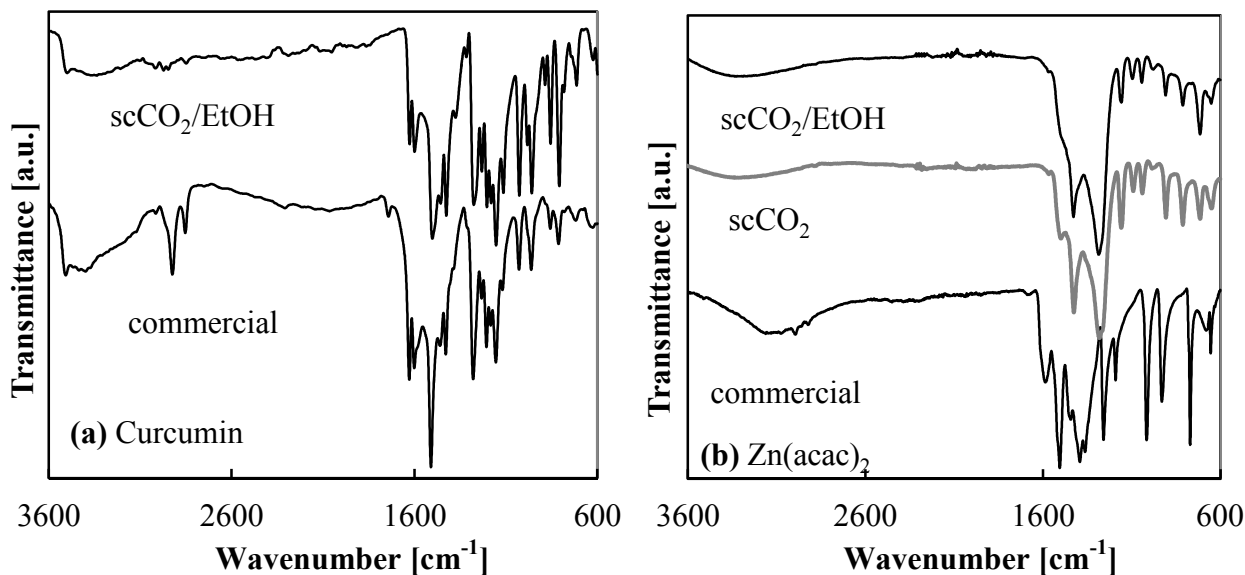


Figure S2. ATR-FTIR characterization of products and reagents before and after supercritical treatment: (a) CCM, and (b) $\text{Zn}(\text{acac})_2$.

FTIR spectroscopy was used to check if the transformation of $\text{Zn}(\text{acac})_2$ into ZnO took place in the supercritical studied system (Fig. S3). Samples from a control test were analyzed by FT-IR spectroscopy up to 400 cm^{-1} , since ZnO is characterized by a broad band centered at *ca.* 450 cm^{-1} . In this region, The $\text{Zn}(\text{acac})_2$ displayed a sharp band at *ca.* 430 cm^{-1} corresponding to Zn-O stretching. The broad band assigned to ZnO was only observed for the sample obtained in the presence of scCO_2 plus EtOH, and not for the sample processed exclusively with scCO_2 . The $\text{Zn}(\text{acac})_2$, as a reactive metal chelate, is susceptible of the attack of protic solvents. Under solvothermal conditions, the mechanism of $\text{Zn}(\text{acac})_2$ conversion into ZnO relies on the nucleophilic attack of the alcohol to the carbonyl group of the acetylacetonate ligand, followed by the hydrolytic formation of reactive Zn-OH intermediates, which polycondensate forming ZnO. This transformation did not take place in liquid ethanol, but could be favored in the supercritical medium due to the acidity conferred to the ethanol by the CO_2 .

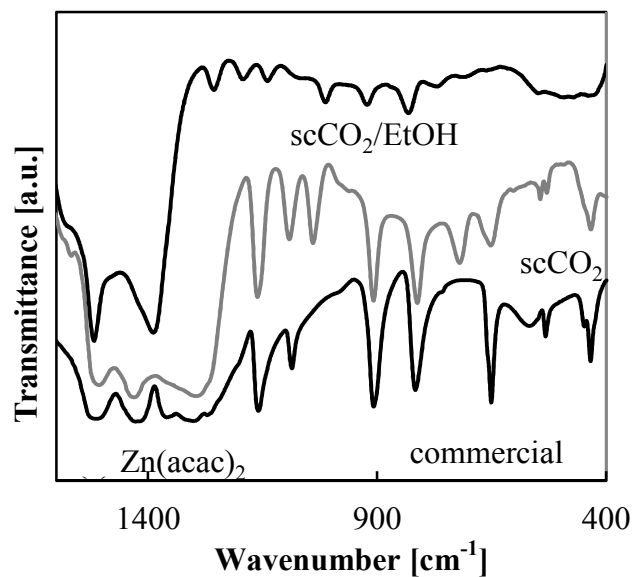


Figure S3. FTIR spectra of raw and treated $\text{Zn}(\text{acac})_2$.

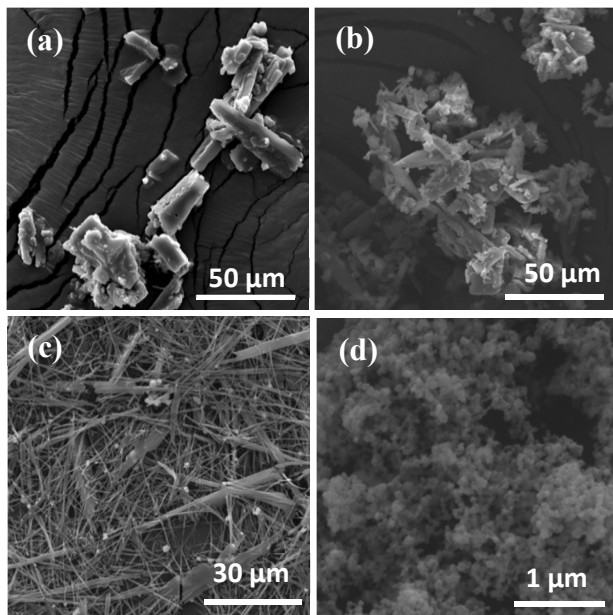


Figure S4. SEM micrographs of the used reagents for MOF synthesis before and after supercritical treatment, for curcumin (a) raw, (b) treated, and $\text{Zn}(\text{acac})_2 \cdot x\text{H}_2\text{O}$ (c) raw, (d) treated.

Crystal growth experiments in EtOH. The reaction between curcumin and $\text{Zn}(\text{acac})_2$ was tested in EtOH in the absence of scCO_2 . The initial mixture of reagents in EtOH was prepared under ambient conditions, resulting in the immediate precipitation of an amorphous solid (Fig. S5 EtOH 298 K pattern), constituted by spherical nanoparticles (Fig. S6a,b). Applying solvothermal heating to this suspension, at either 333 or 353 K in 72 h runs, produced the formation of a crystalline precipitate (Fig. S5 EtOH 333 K pattern). The recorded diffractograms of the powders obtained at both temperatures were similar. However, this pattern did not match either the published phase medi-MOF-1 or the one described in this article as sc-CCMOF-1. The solid was constituted by large ($> 100 \mu\text{m}$) spherical particles with spherulitic habit (Fig. S6c,d).

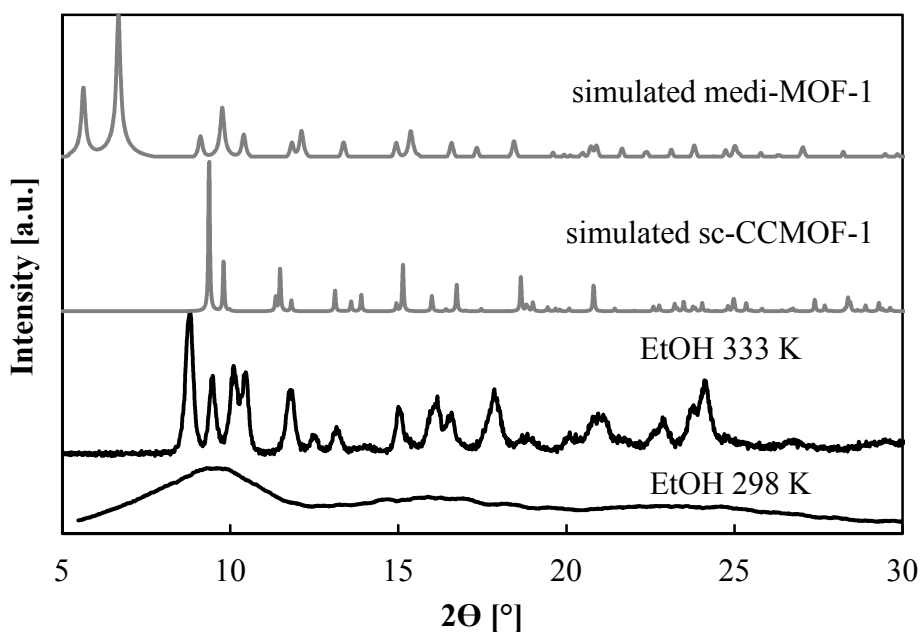


Figure S5. Characterization of the solids precipitated in pure EtOH at different temperatures and running times. Patterns of described Zn/CCM phases are also included for comparison.

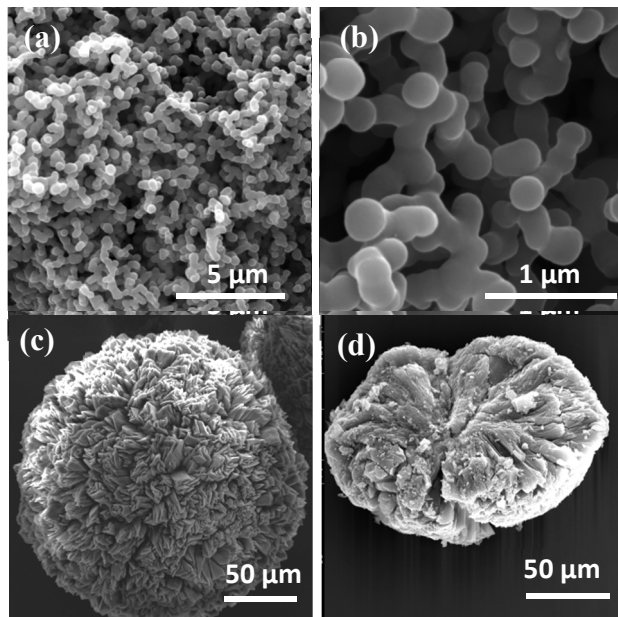


Figure S6. SEM images of the solid particles prepared in EtOH under different experimental conditions: (a,b) nanoparticles obtained at 298 K after 1 h run, and (c,d) microspheres precipitated at 333 K with a crystallization time of 72 h

Single crystal preliminary refinement

Table S1. Structural and EDT experimental details of sc-CCMOF-1.

Crystallographic details	
Formula	Zn(C ₂₁ H ₁₈ O ₆)
Formula weight, g mol⁻¹	431.74
Space group	<i>P2₁/n</i>
<i>a</i>, Å	12.0
<i>b</i>, Å	15.6
<i>c</i>, Å	11.2
α, °	90
β, °	99.6
γ, °	90
<i>V</i>, Å³	2070
N° independent atoms (non-H)	28
EDT data collection and structure determination	
TEM type	Zeiss Libra 120
Accelerat. voltage, kV	120
λ, Å	0.0335
Tilt range, °	100 + 56*
Tilt step, °	1
Data resolution, Å	1.0
Independent reflection coverage, %	94
<i>R</i>_{int}, %	19.33
<i>R</i>_{SIR}, %	33.85

*: the intensity data set was obtained merging two EDT acquisitions obtained from two independent crystals.

Due to the limited quality of the data, the initial structural model showed distorted bond length and angles for the ligand. The addition of soft restraints already allowed to clearly distinguish single and double bonds based on their lengths. The obtained arrangement of single and double bonds was very much consistent with the known structures of curcumin (CCM) in neutral and anionic form.^{1,2} This allowed us to apply more specific geometrical constraints and

restraints based on the literature values, in order to obtain idealized and chemically reasonable ligand geometry. H atoms were placed at idealized positions and refined with a riding model. All changes were supported by improvement in the agreement factors.

Table S2. PXRD experimental parameters summary and Rietveld refinement results.

PXRD data collection and Rietveld refinement	
Diffractometer type	Bragg-Brentano
Radiation	CuK $\alpha_{1,2}$
Average λ, Å	1.5418
2θ range, °	5.0 – 70.0
2θ step, °	0.02
d-spacing resolution, Å	1.343
Refined lattice parameters	
a, Å	12.0164(22)
b, Å	15.5754(13)
c, Å	11.2140(22)
α, °	90
β, °	99.643(9)
γ, °	90
V, Å³	2069.17(24)
Observations	3229
Reflections	896
Refined parameters	60
R_{exp}, %	0.493
R_p, %	3.032
R_{wp}, %	4.129
RF, %	4.195
RF², %	10.081

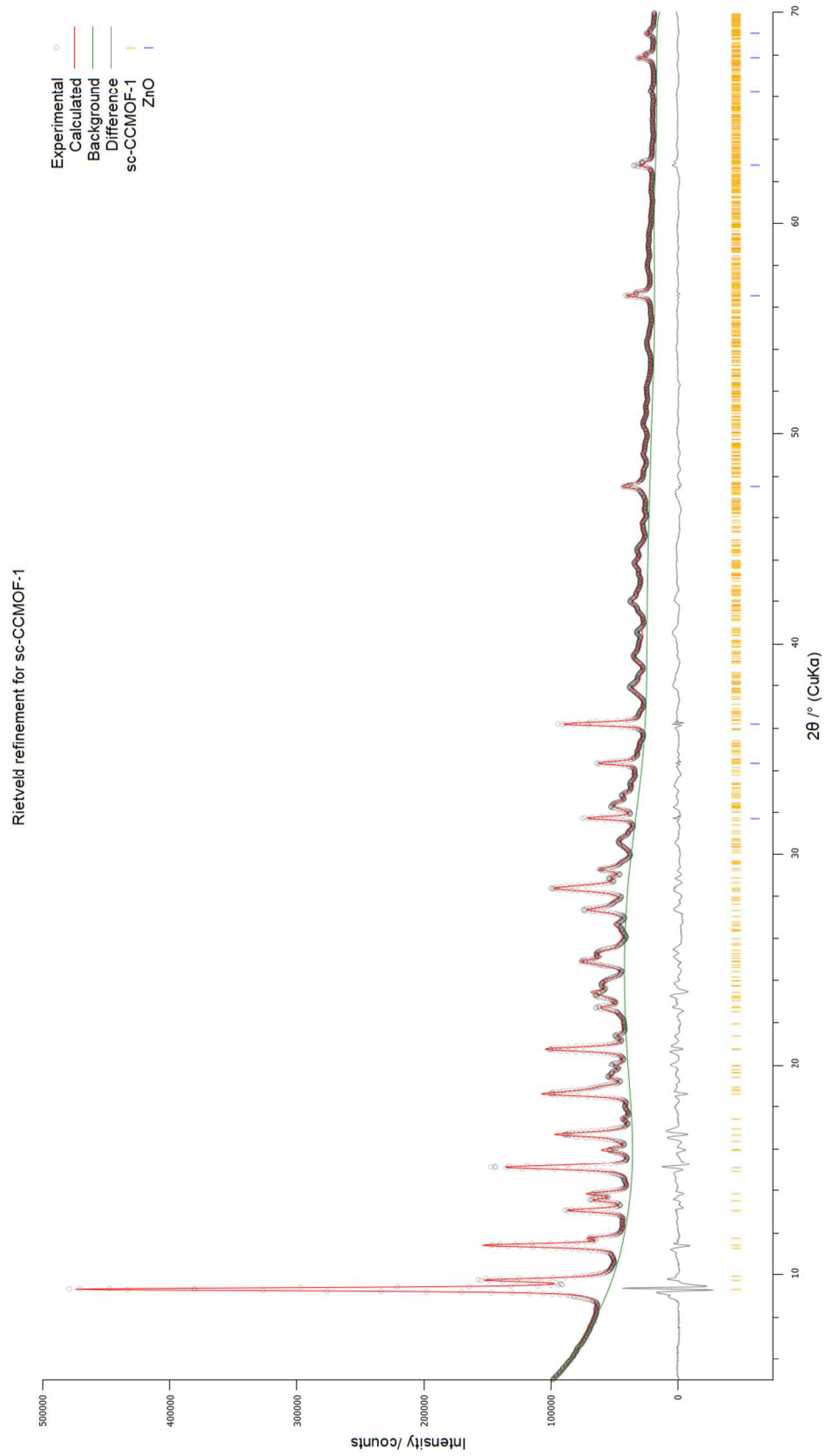


Figure S7. Final Rietveld refinement.

PXRD structure refinement. The pattern showed impurity peaks due to the presence of ZnO.³ Thanks to the much smaller unit cell parameters and high symmetry, the overlap with the phase of interest is minimal and ZnO could be included in the refinement with no detrimental effects and negligible increase in the number of parameters. The refinement was carried out with GSAS-II.⁴ The background was described by fitting manually-picked fixed points with a 24th order Chebyshev polynomial, and it was thereafter kept fixed. Initial pseudo-Voigt profile parameters were empirically refined to obtain a good fit on the ZnO peaks, which were systematically sharper than the sc-CCMOF-1 peaks. The pre-refined single crystal model was used as starting coordinates for the MOF phase. Moreover, a rigid body model for curcumin was created with the programs Mercury⁵ and Avogadro⁶ from the single-crystal coordinates. Selected torsion angles (highlighted in Fig. S8) were set as refineable, allowing for deviations from planarity of the molecule. Then the x, y, z coordinates and U factor were freely refined for Zn, while the position, orientation, overall U factor, and torsion angles were refined for the ligand.

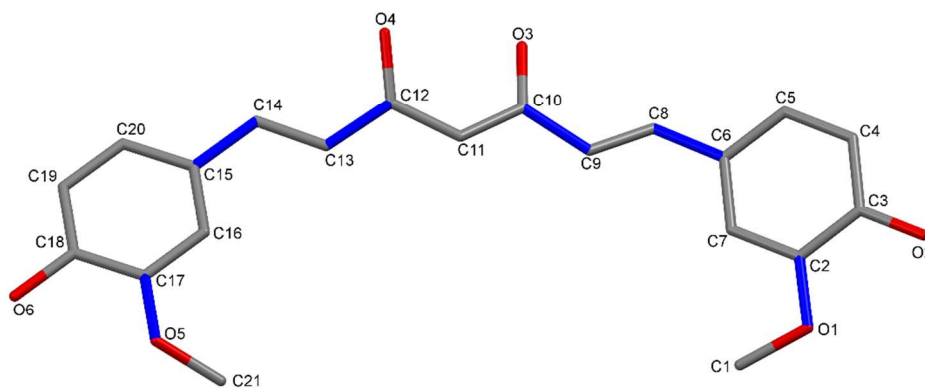


Figure S8. Rigid body model of curcumin. Those torsion angles around the bonds highlighted in blue were set as refineable.

Moreover, additional parameters, including phase fraction, size and strain, and preferred orientation, were refined for both phases to improve the fitting. All variables were alternatively refined until convergence. Finally, C-bonded H atoms were added in calculated positions and final refinement cycles were performed.

Crystal structure

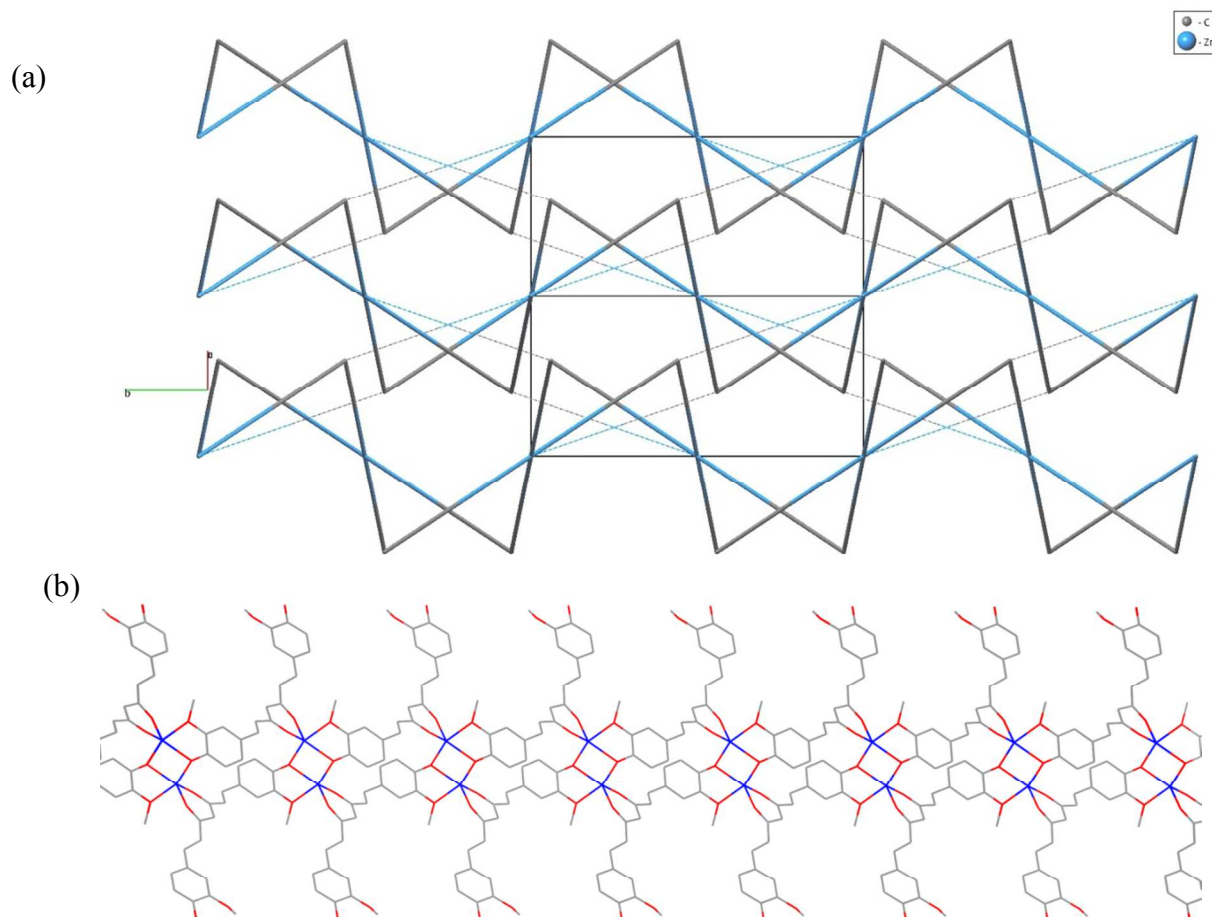


Figure S9. Simplified representation of the crystal structure of the sc-CCMOF-1, (a) viewed along the *b* axis. ZnO_n polyhedra are represented in blue and ligands are represented as grey linkers. By considering only covalent bonds (thick solid lines) the ligand acts as a L-shaped ditopic linker bridging neighboring Zn atoms forming corrugated layers stacked along the *a* axis. Expected hydrogen bonds (thin dashed lines) cross link the layers forming a non-covalent 3D framework, in which the ligands act as T-shaped tritopic linkers; and (b) cross-section view of the layers.

SEM morphological analysis

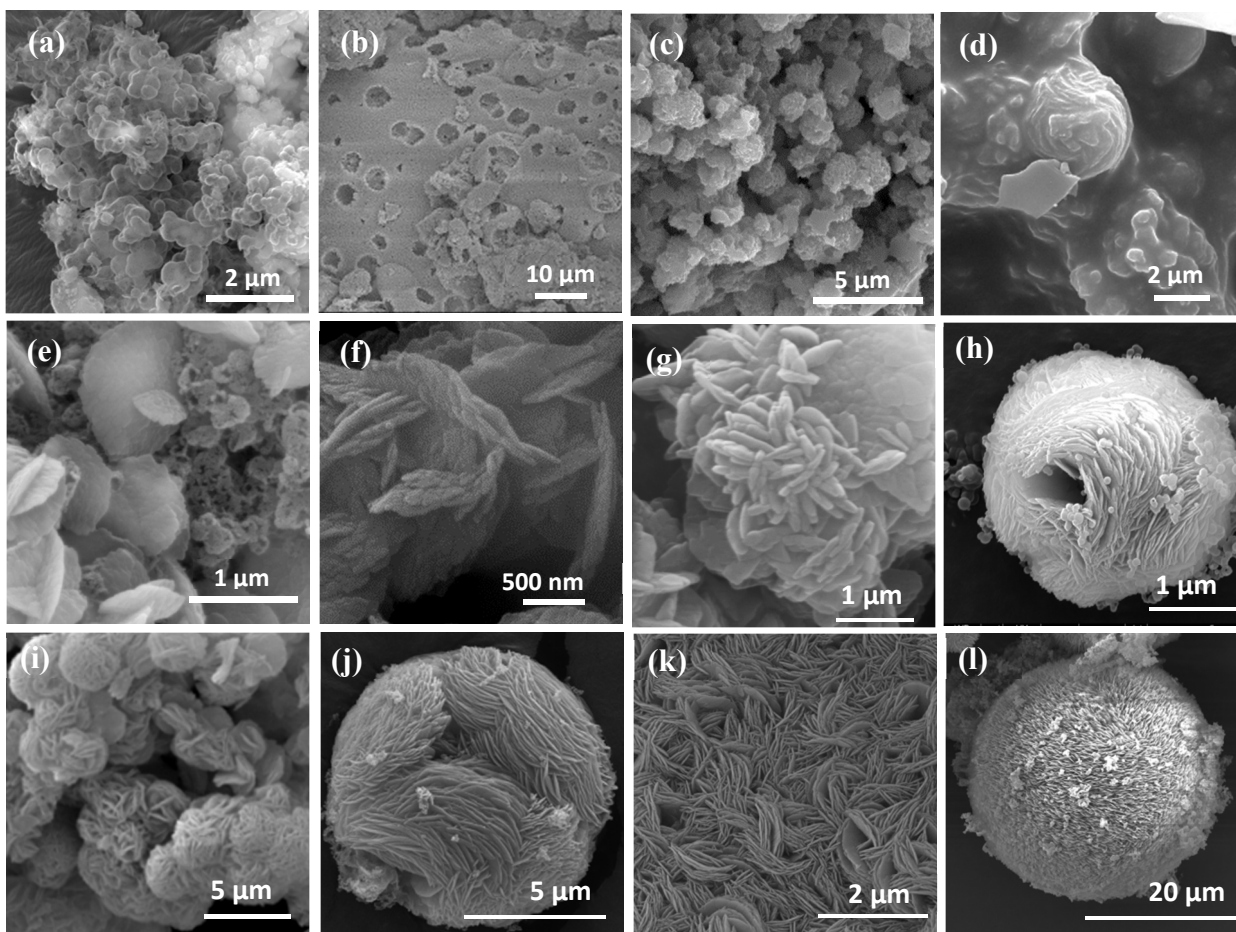


Figure S10. SEM micrographs taken from sc-CCMOF-1 samples prepared following the standard supercritical protocol at different running times: (a,b) 1 h, (c,d) 3 h, (e,f) 10-15 h, (g,h) 20 h, (i,j) 20-72 h, and (k,l) 72-168 h.

References

1. Tønnesen, H. H., Karlsen, J. & Mostad, A. Structural Studies of Curcuminoids. I. The Crystal Structure of Curcumin. *Acta Chemica Scandinavica B* **36**, 475–479 (1982).
2. Su, H., Sun, F., Jia, J., He, H. & Wang, A. A highly porous medical metal – organic framework constructed from bioactive curcumin. *Chem. Commun.* **51**, 5774–5777 (2015).
3. Kihara, K. & Donnay, G. Anharmonic thermal vibrations in ZnO. *Can. Mineral.* **23**, 647–654 (1985).
4. Toby, B. H. & Dreele, R. B. Von. GSAS-II : the genesis of a modern open-source all purpose crystallography software package. 544–549 (2013).
doi:10.1107/S0021889813003531
5. Macrae, C. F. *et al.* Mercury CSD 2.0 - new features for the visualization and investigation of crystal structures. *J. Appl. Crystallogr.* **41**, 466–470 (2008).
6. Avogadro: an open-source molecular builder and visualization tool. <http://avogadro.cc/>.